Water Research 240 (2023) 120063

Contents lists available at ScienceDirect

Water Research

journal homepage: www.elsevier.com/locate/watres

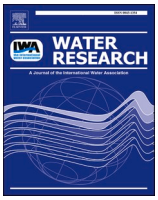

# Hypoxia formation triggered by the organic matter from subsurface chlorophyll maximum in a large estuary-shelf system

Dou Li [a], Jianping Gan [a,*], Zhongming Lu [a], Weicong Cheng [a], Hiusuet Kung [a], Junlu Li [b]

[a] Center for Ocean Research in Hong Kong and Macau, Department of Ocean Science and Department of Mathematics, Hong Kong University of Science and Technology, Hong Kong, China
[b] Department of Earth, Ocean and Atmospheric Sciences, Hong Kong University of Science and Technology (Guangzhou), China

ARTICLE INFO

*Keywords:*
Subsurface chlorophyll maximum
Hypoxia
Frontal convergence
Coupled estuary-shelf dynamics

ABSTRACT

This study reports, for the first time, the role of shoreward transport of organic matter (OM) from subsurface chlorophyll maximum (SCM) in triggering hypoxia off the Pearl River Estuary (PRE, an outstanding example of typical estuary-shelf systems) based on field measurements. Compared to frequently observed hypoxia driven by surface eutrophication and terrestrial OM during large river discharge, we demonstrate that the upslope-transported SCM played a critical role in forming offshore hypoxia during low river discharge. Together with the plume-sourced OM trapped below the surface plume front, upslope-transported OM originating from the SCM accumulated underneath the pycnocline and consumed dissolved oxygen (DO), enhancing the bottom hypoxia. The DO consumption induced by the SCM-associated OM was estimated to contribute ~ 26% (±23%) of the DO depletion under the pycnocline. Based on coherent and consistent physical and biogeochemical evidence and reasoning, this study reveals the contribution of SCM to bottom hypoxia off the PRE, which is unreported and likely occurs in other coastal hypoxic systems.

## 1. Introduction

Hypoxia in aquatic ecosystems is typically defined as dissolved oxygen (DO) less than 2 mg/L. It has been reported in more than 400 coastal waters (Diaz and Rosenberg 2008), where it has significant impacts on organisms and the ecosystem (Breitburg et al. 2018). The classic paradigm for hypoxia formation in estuaries, coastal waters, and marginal seas is that, under favorable hydrodynamic conditions, anthropogenic nutrient input stimulates surface eutrophication and thus exacerbates bottom oxygen depletion (Fennel and Testa 2019).

Located in the northern South China Sea (NSCS, Fig. 1), the Pearl River is the 17th largest river globally, with a mean discharge of 14198 $m^3/s$ during the wet season (June to August). The circulation in summer around the Pearl River Estuary (PRE) is driven by the buoyant plume and upwelling favorable winds. Persistent upwelling circulation exists over the shelf in response to upwelling favorable wind caused by the westward along-isobath pressure gradient force and bottom friction. The upwelling circulation is largely sustained during episodic downwelling favorable winds except in the shallow nearshore regions (Gan et al. 2009, Gan et al. 2015, Liu et al. 2018). The convergent circulations induced by cyclonic vortices enhance the stratification, prolong residence time and accumulate nutrients and organic matter (OM), making the coastal transition zone a favorable environment for bottom hypoxia (Li et al. 2020). Surface eutrophication is the main driver of hypoxia in the PRE, contributing 65% (±16%) of the oxygen-consuming OM, with terrestrial OM accounting for the rest (35%±16%) (Qian et al. 2017, Su et al. 2017, Yu et al. 2021). However, we observed bottom hypoxia in the offshore regions beyond the coverage of surface plume water; in those regions, plume-induced OM, including marine OM from surface eutrophication and terrestrial OM, are limited because of the low river discharge during and before the cruise period (Fig. 2a). Moreover, such a low river discharge during the cruise is unfavorable for hypoxia (Li et al. 2021, Yu et al. 2021). The current understanding of hypoxia formation off the PRE driven by plume-induced OM cannot fully explain the observed severe hypoxia in this study.

Originating from the interactions between ecosystem and hydrodynamics in stratified waters, the subsurface chlorophyll maximum (SCM) is the highest concentration layer of chlorophyll (Chl-a) occurring at a certain depth below the sea surface (Cullen 2015, Yasunaka et al. 2021). Its contribution to photosynthesis and OM supplement makes SCM a significant player in biogeochemical cycles (Garcia-Robledo et al. 2017). The SCM, varying spatiotemporally, affects the distribution of primary

* Corresponding author.
*E-mail address:* magan@ust.hk (J. Gan).

https://doi.org/10.1016/j.watres.2023.120063
Received 22 December 2022; Received in revised form 8 May 2023; Accepted 9 May 2023
Available online 15 May 2023

production, particulate organic matter (POM), dissolved organic matter (DOM), and consequently, DO (Kessouri et al. 2021, Sathyendranath et al. 2009, Xing et al. 2014, Yasunaka et al. 2021). The SCM has been frequently observed over the coastal shelf in the NSCS, coupled with high concentrations of the POM and DOM (Chen and Zhao 2021, Wu et al. 2017, Xing et al. 2019). The SCM is expected to be less likely to affect estuarine waters because it is generally observed in deep waters at a depth of ~50 m where stratification exists and nutrients are available in the NSCS (Lu et al. 2010). However, our recent observations show that high concentrations of OM originating from the SCM were transported upslope towards the PRE by persistent coastal upwelling circulation. Previous studies showed that the relationship between Chl-a and POM is constant in diatom-dominated waters (Gardner et al. 2006), which is also the dominant group near the PRE (Huang et al. 2004, Xu et al. 2022). A power-law function between POM and Chl-a concentration off the PRE (Wang et al. 2011) is proved to be consistent with the result listed by Sathyendranath et al. (2009). The SCM has been reported in coastal waters such as the Gulf of Mexico (Pasqueron de Fommervault et al. 2017) and Changjiang Estuary (Lee et al. 2017), which would fuel hypoxia when the phytoplankton in the SCM dies and sinks to the bottom. However, the contribution of the OM from the SCM to hypoxia has never been discussed in such estuarine hypoxic systems. In this manuscript, we provide observational evidence and quantify the contribution of the OM from the SCM to the hypoxia off the PRE, a representative of large estuaries.

## 2. Materials and methods

### 2.1. Study region and cruise background

In the framework of OCEAN-HK (Ocean Circulation, Ecosystem and hypoxiA arouNd Hong-Kong waters, https://ocean.hkust.edu.hk/) project, a total of fourteen cruise surveys were conducted in the PRE and adjacent NSCS shelf waters during the summers of 2014 to 2021 (Table S1 and Fig. 1b). This study focuses on the repeated cross-shelf transects, P3 to F7, extending from nearshore to the 30m isobath sampled on 29-30 August 2021 (2021-L3, magenta circles in Fig. 1b). During the cruise period of 2021-L3, downwelling favorable wind prevailed with an alongshore wind stress of 0.026 Pa. The river discharge was relatively low (~2409 $m^3/s$), only 17% of the summer average.

### 2.2. Sampling and data processing

In situ salinity and temperature were measured by a Sea-Bird SBE19plus Conductivity–Temperature–Depth (CTD) profiling system with a precision of 0.00007 S/m and 0.0001 °C. Chl-a and nitrate ($NO_3$) were measured with additional chlorophyll fluorescence and SUNA sensors with a detection limit of 0.016 $\mu$g/L and 0.5 $\mu$M, respectively. The resolution for optical dissolved oxygen sensor is 0.007 mg/L. For accuracy, water samples at the surface (~1m), middle and bottom layers (~3m above the bottom) were collected from free-flow water samplers mounted onto a Rosette sampling assembly for calibration of the Chl-a, DO, and $NO_3$ from sensors. Concentrations of Chl-a in discrete samples were determined by a Turner Designs fluorometer after extracting filters with 90% acetone at -20°C (Zhao et al. 2020), and DO were measured onboard using the spectrophotometric Winkler method with a precision of 0.03 mg/L (Dai et al. 2006). Nutrient samples were run with a Technicon AA3 Auto-Analyzer with a detection limit of 0.1 $\mu$M. Dissolved organic carbon (DOC) concentration was determined by a total organic carbon (TOC) analyzer (Shimadzu TOC-V CPH), following the processes described in Wu et al. (2015), and the coefficient of variation of replicate measurements was approximately 2%. The samples were analyzed for particulate organic carbon (POC) using a PE-2400 SERI II CHNS/O analyzer with the precision <10% described previously (Li et al. 2018, Wu et al. 2015, Wu et al. 2017). We interpolated the calibrated data from CTD sensors into a mesh grid with a resolution of 0.01 degrees to depict the surface and bottom horizontal distribution. The data are also interpolated vertically with a resolution of 0.2m to show their vertical characteristics.

To support our analysis, we used the daily river discharge rate from the Information Center of Water Resources (http://xxfb.mwr.cn/sq_djdh.html). Hourly wind data in Wagland Island (WGL) were obtained from the Hong Kong Observatory (https://eforms.weather.gov.hk/eforms_v2/online_reqform_e.fm). Averaged river discharge and wind stress were calculated during the cruise period to indicate the hydrodynamic conditions (Table S1). We used surface Chl-a satellite data with a resolution of 5 km provided by the Japan Meteorological Agency (JMA, https://www.eorc.jaxa.jp/ptree/index.html) to check the Chl-a distribution before and during the cruise.

## 3. Results

### 3.1. Observed SCM and hypoxia

During the cruise period of 2021-L3, a northeasterly wind prevailed, and the river discharge was relatively low (~2409 $m^3/s$), which was only 17% of the summer average. The plume fronts and surface eutrophication were confined to the coastal regions shallower than 20m,

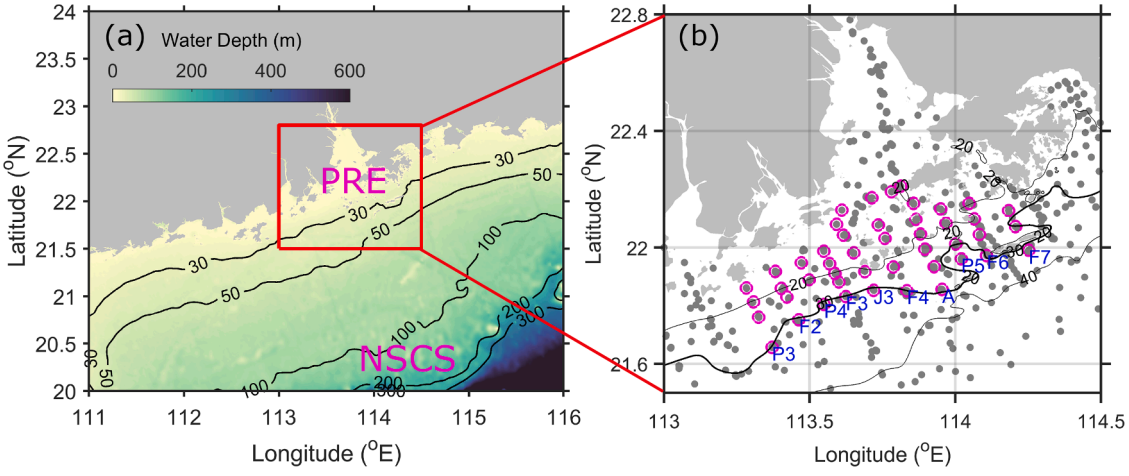


**Fig. 1.** (a) Bathymetry of the study area in the PRE and adjacent shelf waters, and (b) sampling stations for fourteen cruises during the summer of 2014 to 2021 (gray dots). Magenta circles highlight the sampling stations during 2021-L3. The black lines are the 30, 50, 100, 200, and 300m isobaths in (a) and the 20, 30, and 40m isobaths in (b).

according to both the field observations and the JMA satellite data (Fig.s 2a and b). We observed bottom hypoxia (Fig. 2a) over an area of ~387 $km^2$ of the shelf between the 20m and 30m isobaths, which is beyond the hypoxia area induced by plume-induced OM according to historical observations and numerical simulations (Li et al. 2021, Yu et al. 2021). Furthermore, and of particular note, the hypoxia occurred on the offshore side of the plume region, where SCM reached (Fig. 2b). The hypoxia accompanied by the SCM that we observed in a large estuary has not been reported before, and it raises the question of what role the SCM plays in the formation of bottom hypoxia.

The vertical distributions of physical and biogeochemical variables along cross-shore sections showed that the SCM contributed to the hypoxia formation (Fig. 3). The offshore-generated SCM and associated OM were transported onshore by persistent upslope upwelling circulation and accumulated in the bottom confluent zones at the edge of the plume where the SCM intersected the sloping topography. Consequently, the SCM with Chl-a>2 μg/L was observed at a depth between 15m and 25m (referred to as the SCM layer hereafter) along these cross-shore transects. The linkage between SCM and upslope transport is shown by the large $N^2$ where sub-pycnocline existed (~20m depth, Fig. 3g-i). Affected by the terrestrial input and plume-induced eutrophication, the POC and DOC (dots in Fig. 3a-f) were high within the plume regions and decreased offshore due to dilution, degradation, and decreasing surface primary production (Li et al. 2018, Wu et al. 2017). Meanwhile, a relatively higher concentration of POC was found within the SCM layer and decreased sharply with depth, while the DOC was not obviously higher in the SCM layer due to our low sampling resolution. The existence of local sub-pycnocline and enrichment of OM from SCM provided favorable conditions for the formation of the hypoxia along Sections F2, P4, and F3 (Fig. 3d-f).

Apart from the cross-shore sections, the vertical distributions of Chl-a, $N^2$, DO, and $NO_3$ along the 30m-isobath provide more direct evidence for the SCM occurrence and its contribution to hypoxia formation (Fig. 4). A high concentration of Chl-a was observed at the depths of 15m to 25m, with the highest value (5.2 μg/L) at the western PRE near F204 (Fig. 4a). This higher concentration was related to the enhanced cross-shore upwelling, as shown by stronger $N^2$ and colder bottom water (Fig. 4b and S3). Correspondingly, we observed higher concentrations of POC and DOC within the SCM layer (dots in Fig. 4a and c), except that DOC peaked at the surface for plume-affected stations (i.e., F204, P403, and F305). Remineralization beneath the pycnocline led to a decrease in DO (Fig. 4c) and an increase in $NO_3$ (Fig. 4d) at the bottom. Higher Chl-a and lower DO in the SCM layer were found in the western part of the section. The spatial differences in the SCM and DO distribution support the conclusion that the DO decline was positively related to the Chl-a concentration within the SCM layer during the cruise of 2021-L3.

To further support our conjecture, we calculated the correlation between the minimum DO and maximum Chl-a in the subsurface (deeper than 15m) at the depth of 30m with a total of 155 samples from the fourteen cruises (Fig. 5a). We found that minimum DO is negatively correlated with the subsurface Chl-a maximum with R=-0.42 ($p<0.001$), indicating that SCM and associated OM contribute to the DO consumption, although variable physical and biogeochemical processes among different stations make R less than 1. Data from 2021-L3 highlighted by the blue dots generally follow the trend.

### 3.2. *Quantification of the SCM's Contribution*

Although it is not yet possible to directly quantify the in situ oxygen consumption caused by the SCM-associated OM due to limited observations, the empirical relationship of Chl-a and DO differences between stations with SCM (referred to as SCM-stations, n=43) and without SCM (referred to as no-SCM-stations, n=112) selected from historical cruise data (Cruise Numbers 1 to 13 listed in Table S1) can be used to estimate the potential DO consumption during Cruise 2021-L3.

Fig. 5b-c shows the averaged profiles of Chl-a and DO at different stations. Red and magenta lines indicate the averaged profiles of SCM-stations along the 30m and 40m isobaths (referred to as 30m-stations and 40m-stations), respectively. Blue and cyan lines indicate the profiles of no-SCM-stations at 30m-stations and 40m-stations, respectively. The averaged profiles of 2021-L3 (Cruise Number 14 in Table S1) at 30m-stations are shown separately by the green lines (referred to as SCM-2021-L3). Contrasting with the no-SCM-stations where Chl-a peaked at the surface, for SCM-stations, the maximum Chl-a appeared at the sub-pycnocline or in benthic water (Fig. 5b). The SCM was stronger for the 30m-stations than the 40m-stations, primarily because the enriched nutrients enhanced the SCM and the upslope-transported SCM accumulated in the nearshore regions (Chen and Zhao 2021, Li et al. 2020). The DO depletion through remineralization exceeded the DO supply through photosynthesis and vertical mixing, leading to lower DO within the SCM layer (Fig. 5c). Moreover, DO was higher at 40m-stations than at 30m-stations (Fig. 5c), confirming that local intensified DO consumption is the dominant factor of hypoxia formation, rather than onshore advection of low DO water. The averaged profiles of the

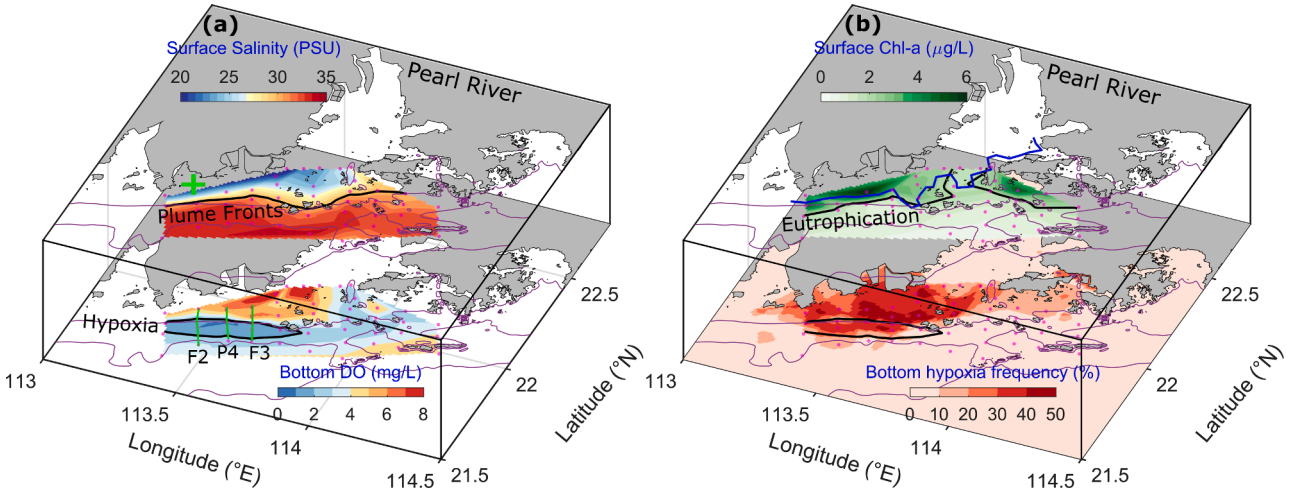


**Fig. 2.** Horizontal distribution of (a) surface salinity and bottom DO of Cruise 2021-L3, (b) surface Chl-a of 2021-L3 and bottom hypoxia frequency (the ratio between hypoxia occurrence and total cruises listed in Table S1). The magenta dots represent sampling locations, and the data are interpolated into a mesh grid with a resolution of 0.01 degrees. The black lines in (a-b) show salinity=30 PSU, DO=2 mg/L or hypoxia, Chl-a=2 μg/L, respectively. Purple lines indicate the 20, 30, and 40m isobaths. The green cross in (a) shows the buoy location. The blue line in (b) shows Chl-a=2 μg/L of JMA satellite data averaged from 29 to 30 August 2021.

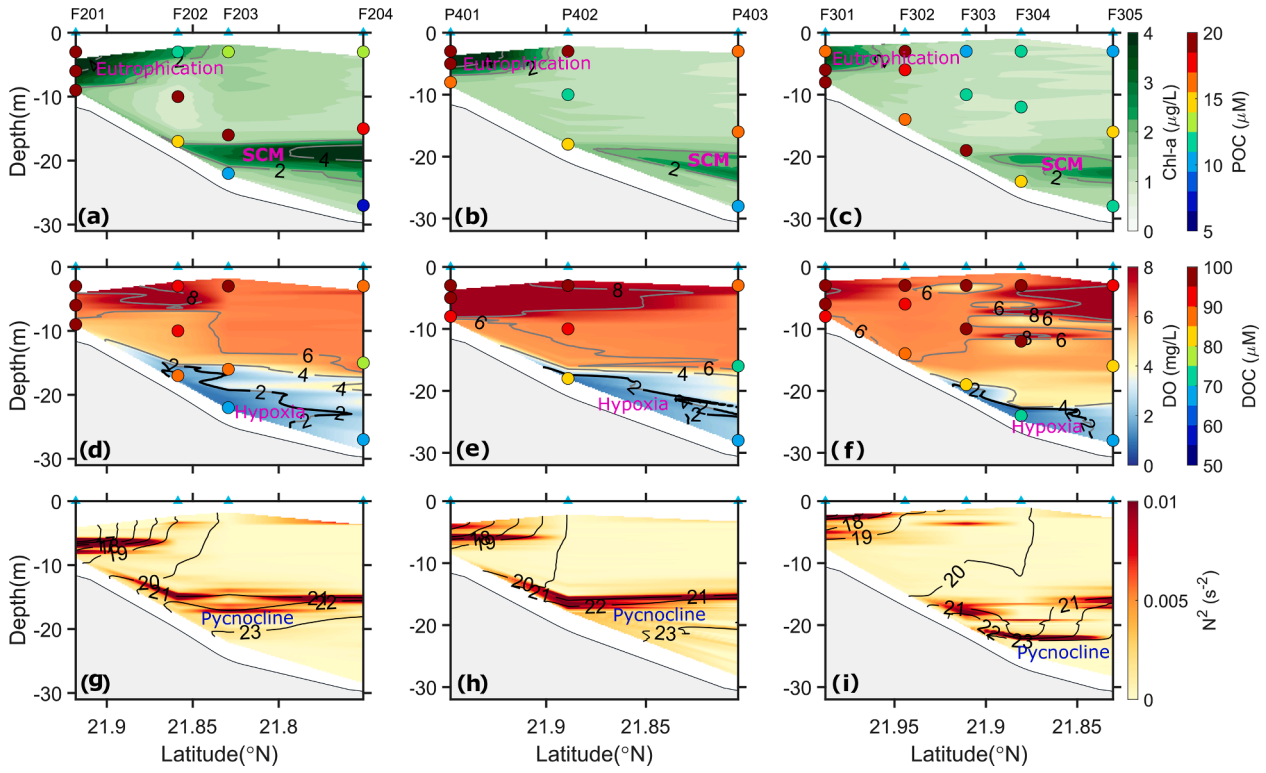


**Fig. 3.** Vertical distribution of (a-c) Chl-a and POC (dots), (d-f) DO and DOC (dots), (g-i) square of buoyancy frequency ($N^2$) along Section F2 (left panel), P4 (middle panel), and F3 (right panel) of 2021-L3 shown by green lines in Fig. 2a.

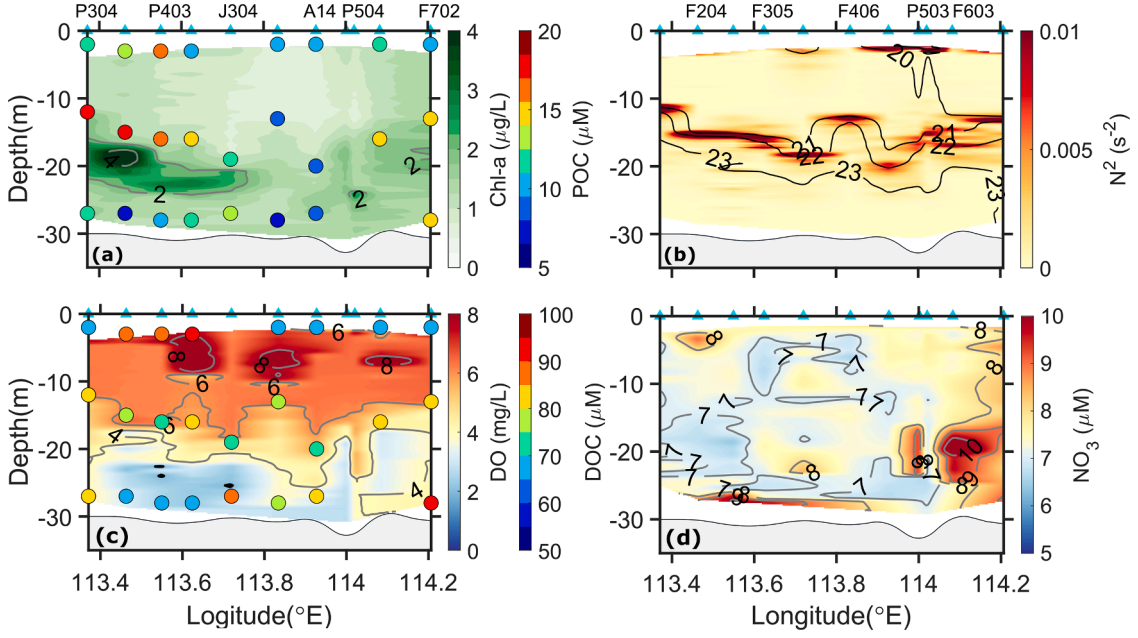


**Fig. 4.** Vertical distribution of (a) Chl-a and POC (dots), (b) square of buoyancy frequency ($N^2$, colored) and density (contour lines), (c) DO and DOC (dots), and (d) $NO_3$ of stations (n=11) during 2021-L3 along the 30m-isobath shown in Fig. 1.

SCM-2021-L3-stations (green lines) resembled the SCM-30m-stations (red lines). However, the bottom DO was much lower or reached hypoxia at some stations, although the Chl-a was less than SCM-30m-stations (Fig. 5b-c).

The impact of SCM on DO depletion can be quantified by examining the difference of the averaged Chl-a and DO profiles between SCM and no-SCM stations, under the consideration that the DO fluxes induced by physical and biogeochemical processes are consistent and have a small difference between SCM and no-SCM stations in the averaged results. Thus, the difference of the averaged Chl-a and DO profiles between these two kinds of stations has excluded or non-SCM effect is minimized. We also adopted the previous findings that the ratio between Chl-a and DO consumption is constant in the diatom-dominant PRE (Sathyendranath et al. 2009, Wang et al. 2011). Upon these considerations, we compared

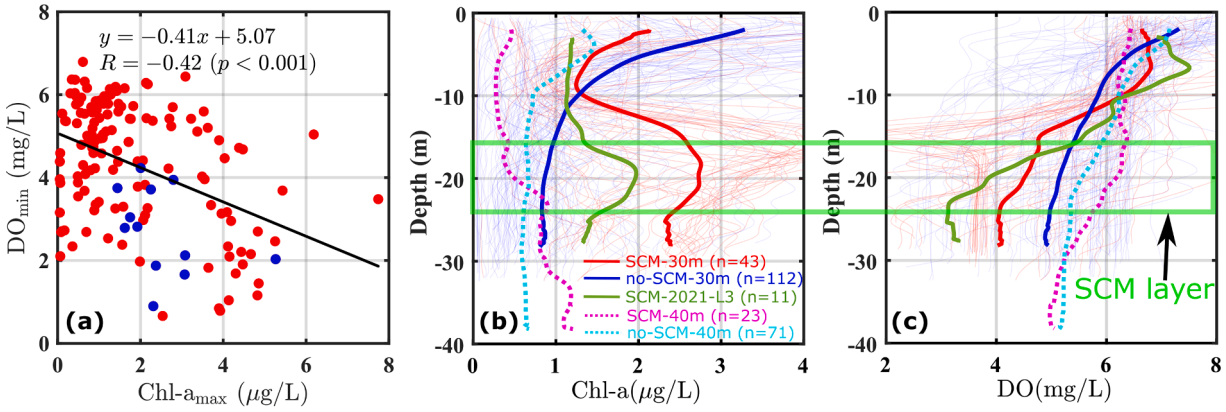


**Fig. 5.** (a) Correlation between the minimum DO and maximum Chl-a in the subsurface (deeper than 15m) for 30m-stations among cruises listed in Table S1. Data from 2021-L3 is highlighted by the blue dots. Averaged vertical profiles of (b) Chl-a, and (c) DO among stations with and without SCM along the 30m (solid lines) and 40m (dashed lines) isobaths with n showing the number of stations collected from 2014 to 2021. The averaged profiles of SCM-2021-L3-stations along 30m-isobath (shown in Fig. 4) are shown separately by the green lines. The thin lines show the original sampling profiles at each station along the 30m-isobath. The green square indicates the SCM layer.

the averaged Chl-a and DO profiles of the SCM-stations and SCM-2021-L3 with no-SCM-stations and calculate their depth-integrated values below the pycnocline (deeper than 15m, Fig. 6a-b). The difference shows that Chl-a difference (ΔChl-a) ranging from 1.47~1.89 μg/L and associated OM led to a decrease of 0.56~0.92 mg/L in DO (ΔDO) below the pycnocline for the SCM-30m-stations (magenta lines in Fig. 6a-b). The depth-integrated DO consumption ($\Delta DO_{int}$) beneath the pycnocline reached 9.29 g/m$^2$ (cyan dashed line), mainly attributed to the enrichment of Chl-a induced by SCM ($\Delta Chl\text{-}a_{int}$ =21.03 mg/m$^2$, cyan dashed line). In other words, the relationship between $\Delta Chl\text{-}a_{int}$ (mg/m$^2$) and $\Delta DO_{int}$ (g/m$^2$) based on 155 samples from repeatedly sampling stations in the 13 cruises is

$$\langle \Delta DO_{int} \rangle = -0.44 \langle \Delta Chl\text{-}a_{int} \rangle, \quad (1)$$

here $\langle \cdot \rangle$ means the averaged result of historical cruise data, and subscript int refers to the depth integration below the pycnocline. Although oxygen dynamics are regulated by many processes, such as the remineralization rate of the OM, residence time, horizontal advection, vertical mixing, etc., differences in DO fluxes induced by these processes are excluded or minimized in the averaged profiles for SCM and no-SCM stations. Besides, $\Delta DO_{int}$ and $\Delta Chl\text{-}a_{int}$ are significantly correlated with R=-0.36 ($p<0.05$, Figure not shown). Therefore, the averaged relationship between $\Delta Chl\text{-}a_{int}$ and $\Delta DO_{int}$ (Equation 1) is practical to estimate the contribution of SCM to hypoxia, that is,

$$\begin{aligned} \text{Contribution} &= \frac{\Delta Chl\text{-}a_{int}}{\Delta DO_{int}} \times \frac{\langle \Delta DO_{int} \rangle}{\langle \Delta Chl\text{-}a_{int} \rangle} \times 100\% \\ &= -0.44 \frac{\Delta Chl\text{-}a_{int}}{\Delta DO_{int}} \times 100\%. \end{aligned} \quad (2)$$

Nonetheless, it is important to note that physical and biogeochemical processes exhibited variability in different stations and cruises, and that the differences between SCM and non-SCM stations thus varied accordingly. Compared to SCM-30m-stations, the SCM-2021-L3-stations were characterized by a smaller ΔChl-a with a peak of 1.1 μg/L and a larger ΔDO with a maximum of 1.87 mg/L (red lines in Fig. 6a-b). Thus, the $\Delta Chl\text{-}a_{int}$ was about half (~9.59 mg/m$^2$) of the SCM-30m-stations, but the $\Delta DO_{int}$ reached 16.05 g/m$^2$ (blue dashed lines in Fig. 6a-b), suggesting that SCM-induced OM accounted for 26% (contribution = $\frac{9.59}{16.05} \times 0.44 \times 100\% = 26\%$) of the DO decline under the pycnocline for SCM-2021-L3-stations. This value might be underestimated

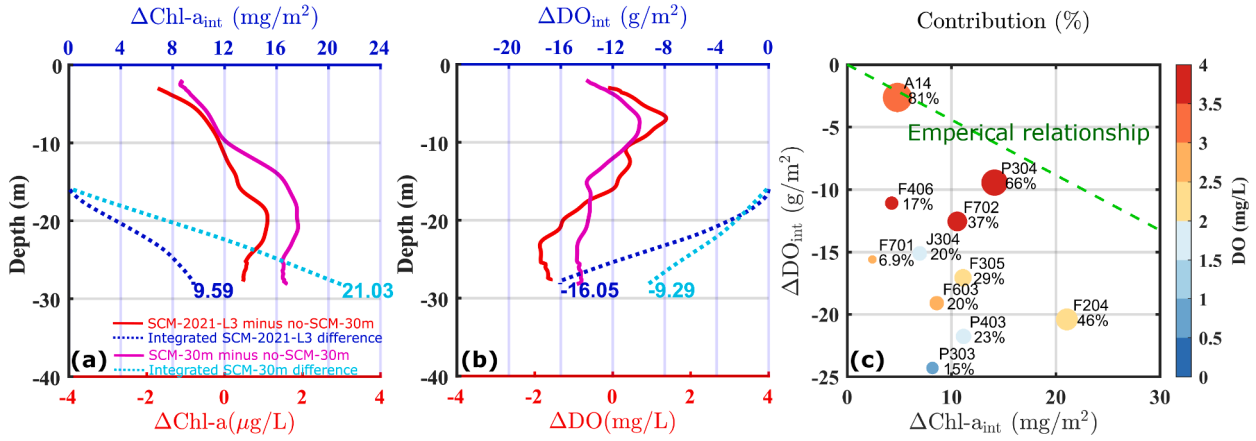


**Fig. 6.** The vertical profiles of (a) Chl-a difference (ΔChl-a) and depth-integrated values ($\Delta Chl\text{-}a_{int}$) below the pycnocline (deeper than 15m), and (b) DO difference (ΔDO) and depth-integrated values ($\Delta DO_{int}$) between the SCM-30m-stations, SCM-2021-L3 and no-SCM-30m-stations (i.e., SCM-30m-stations minus no-SCM-30m-stations, and SCM-2021-L3 minus no-SCM-30m-stations, respectively). (c) The scatter distribution of SCM's contribution calculated from Equation 2 against $\Delta Chl\text{-}a_{int}$ and $\Delta DO_{int}$ with the color showing the minimum DO and the size of dots representing the contribution at SCM-2021-L3-stations. The green dashed line in (c) indicates the empirical relationship between $\Delta Chl\text{-}a_{int}$ (mg/m$^2$) and $\Delta DO_{int}$ (g/m$^2$) calculated from the differences between SCM-30m and no-SCM-30m stations (Equation 1).

considering the relatively weak influence of plume-induced eutrophication during 2021-L3 compared with the general conditions (i.e., no-SCM-30m-stations).

Moreover, the contribution of the SCM to the DO consumption varied among 30m-stations with different minimum DO concentrations during 2021-L3 (Fig. 6c). Specifically, the contribution decreased with the decreasing $\Delta$Chl-$a_{int}$ and $\Delta DO_{int}$ compared to their empirical relationship (Equation 1, green dashed line). Largely determined by the location or distance away from the river plume (shown in Fig. 4a-b), the SCM's contribution ranged from 6.9% at F701 to 81% at A14, with a standard deviation of 23%. Although the contribution of SCM in the hypoxic stations (P303, P403, J304) is less important ($\leq$23%, numbers shown in Fig. 6c from Equation 2) than other DO sinks (e.g., degradation of plume-induced OM in the water column, sediment oxygen consumption, etc.), the presence of the SCM in combination with strong stratification could enhance DO consumption and shift the system from normoxia to hypoxia. An illustration of the significant role of the SCM in triggering hypoxia can be seen at Station P403, where the $DO_{min}$ is measured to be 1.9 mg/L with a contribution of 20% from the SCM (Fig. 6c). If the SCM-induced depletion was removed in $\Delta DO_{int}$ (-15.1 $\times$ 20%=-3.1 g/m$^2$), which corresponds to an increase of 0.2 mg/L in DO at the subsurface. We find that the resulting $DO_{min}$ would be 2.1 mg/L, surpassing the critical level for hypoxia. Similarly, an increase of 0.3 mg/L in DO is found at Station P303 and P403. Such a change would have significant consequences for the aquatic ecological environments.

## 4. Discussion

In situ measurement of DO consumption induced by OM from SCM and river plume (e.g., terrestrial OM, marine OM from surface eutrophication) is challenging. Descriptive statistics are applied to quantify the role of the SCM in hypoxia formation based on data collected from 14 cruises and on our holistic understanding of coupled physical-biogeochemical processes in the region. Two reasonable assumptions or considerations are made to obtain the relationship between Chl-a and DO depletion: 1) DO fluxes induced by physical and biogeochemical processes remain constant in the averaged profiles for SCM and no-SCM stations; 2) the ratio between Chl-a and related DO consumption is constant in PRE. Some uncertainties may arise from the assumptions, but they are expected to be small with justifications by sufficient field data of 155 samples from the 13 cruises and by previous findings. The accuracy of the quantification can be further refined with possible in situ measurement of DO consumption by OM in the SCM.

The river plume can affect the hydrodynamics and biogeochemistry of the estuary-shelf ecosystem. Yet, during our survey in 2021, the plume was confined within the coastal regions with a distinct surface plume front along the 20m-isobath, as mentioned in Section 3.1. The coastally trapped plume and its OM, induced by the episodic downwelling-favorable wind, was not the typical scenario in the summer with the prevailing upwelling-favorable wind. Such a plume front, characterized by convergent flow and a downward velocity, was important for distributing surface Chl-a and OM because it trapped biomass near the frontal convergent zones off the estuaries (Kilcher and Nash 2010, Zhang et al. 2020). The observations also showed a higher concentration of POC below the surface plume front, especially at Stations F202 and F302 (Fig. 3).

The persistent upslope transport in the PRE (Gan et al. 2015) fueled additional OM from the SCM offshore to form the hypoxia, which otherwise might not have occurred with the coastally trapped and weak plume. Fig. 7 summarizes schematically the formation of hypoxia contributed by the OM from the river and the SCM in a large estuary-shelf system. The freshwater and onshore-transported saline water converged near the bottom of plume front. As shown in Fig. 3, this favored the accumulation of terrestrial and autochthonous OM originating from both the surface eutrophication and the SCM. The convergent zones were thus shown to be favorable for hypoxia formation due to

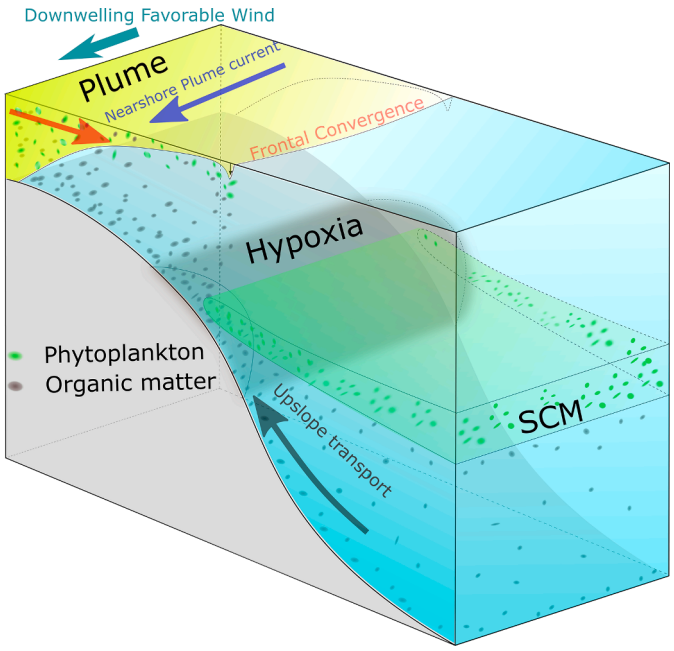


**Fig. 7.** Schematic diagram showing the hypoxia formation contributed by the SCM and associated processes on the seaside of the plume in an estuary-shelf system. The green and gray shadows depict the SCM and hypoxia, respectively. The red and black arrows indicate the flow direction of the plume and upslope transport in the cross-shelf direction. The green dots represent phytoplankton, and the brown dots donate organic matter (OM). The plume-induced surface phytoplankton and terrestrial OM sink to the bottom and accumulate near the front convergent zone. The SCM occurs underneath the pycnocline in both the nearshore and offshore regions and is then transported upslope with OM, which consequently contributes to the formation of bottom hypoxia.

the characteristics of strong stratification and long residence time (Li et al. 2020).

It is also notable that hypoxia was absent in the nearshore coastal regions during 2021-L3, compared to previous observations (Fig. 2b). This is also partly attributed to the low river discharge under the downwelling favorable wind. The plume confined the freshwater within the narrow coastal waters with a deep halocline (Fig. S1c), transported the nutrients to the west, and reduced residence time in the nearshore region. This, together with diminished surface eutrophication, deterred the formation of bottom hypoxia in the plume-affected waters (Li et al. 2021). The variations in salinity, $NO_3$, Chl-a, and DO at depths of 3 m and 6 m (measured from a buoy moored near the western coast, shown by the green cross in Fig. 2a) further confirmed the conclusion (Fig. S1). The salinity decreased and $NO_3$ increased throughout the water column from 25 August when the wind changed from upwelling favorable wind to downwelling favorable wind. The surface Chl-a, which affects surface DO through photosynthesis, decreased after a slight increase due to the short residence time during downwelling favorable wind. The bottom DO varied in the same phase as the surface DO for the enhanced mixing in the shallow coastal regions. Evidently, bottom hypoxia cannot be established for such a short residence time and enhanced vertical mixing under downwelling favorable wind, despite the high POC and DOC in the plume-influenced nearshore region.

This study firstly reports the contribution of the OM from SCM to triggering hypoxia under physical conditions that are not favorable for plume-induced eutrophication and hypoxia. Based on coherent evidence from multiple observations and consistent physical and biogeochemical reasoning, this study enriches our understanding of the mechanisms for coastal hypoxia formation. The presence of the SCM, in combination with strong stratification, could shift the system from normoxia to hypoxia and significantly affect biogeochemical cycles and ecosystems

in the coastal waters off the PRE, which likely occurs in other hypoxic regions (Cullen 2015, Márquez-Artavia et al. 2019, Medina-Silva et al. 2018). Reductions in nutrient loads have improved oxygen conditions in some estuarine hypoxic systems where surface eutrophication is a dominant factor (Kemp et al. 2009). However, hypoxia has not been diminished by management efforts in many other areas, especially in coastal systems where the SCM might contribute to hypoxia formation (Pasqueron de Fommervault et al. 2017, Wang et al. 2019).

## 5. Conclusions

We report the presence of the SCM off the PRE in August 2021 and examine the SCM's contribution to hypoxia formation based on the data from 14 historical cruises conducted from 2014 to 2021. Our result shows that the SCM and associated oxygen consumption by the SCM-derived OM contributed to the unique hypoxia formation under low river discharge and coastally trapped plume due to downwelling favorable wind conditions. The SCM and associated OM are carried onshore by persistent upslope transport over the adjacent shelf and accumulate at the convergent zone of the plume front; this zone is characterized by stable water columns and long residence time. Based on the observationally derived relationship between depth-integrated Chl-a and DO difference under the pycnocline, the DO consumption induced by the SCM-related OM is estimated to contribute an average of 26% (±23%) to the observed DO decline, ranging from 6.9% to 81% for SCM-2021-L3-staions along the 30m-isobath. Moreover, the hypoxia accompanied by the SCM is located at a depth between 20m and 30m on the offshore side of the surface river plume and eutrophication, which indicates the necessary contribution of SCM to the formation of hypoxia when riverine OM and other processes of DO consumption alone are not sufficient for the formation. This study provides new and insightful information for understanding the formation of hypoxia in estuary-shelf systems.

## Declaration of Competing Interest

The authors declare that they have no known competing financial interests or personal relationships that could have appeared to influence the work reported in this paper.

## Data availability

Data will be made available on request.

## Acknowledgements

This work was supported by the Theme-based Research Scheme (T21-602/16-R, OCEAN_HK project) of the Hong Kong Research Grants Council. We are grateful for DOC and POC data provided by the group of Minhan Dai from Xiamen University and the assistance of crew members of *RV Haijian 203*. The Center for Ocean Research in Hong Kong and Macau is a joint research center between Qingdao National Laboratory of Marine Science and Technology and Hong Kong University of Science and Technology. The observed data used in this research can be downloaded from the OCEAN-HK Data and Modeling Server (https://ocean.ust.hk/data/?page_id=670).

## Supplementary materials

Supplementary material associated with this article can be found, in the online version, at doi:10.1016/j.watres.2023.120063.

## References

Breitburg, D., Levin, L.A., Oschlies, A., Gregoire, M., Chavez, F.P., Conley, D.J., Garcon, V., Gilbert, D., Gutierrez, D., Isensee, K., Jacinto, G.S., Limburg, K.E., Montes, I., Naqvi, S.W.A., Pitcher, G.C., Rabalais, N.N., Roman, M.R., Rose, K.A., Seibel, B.A., Telszewski, M., Yasuhara, M., Zhang, J., 2018. Declining oxygen in the global ocean and coastal waters. Science 359 (6371).

Chen, Y., Zhao, H., 2021. Spatial distribution of the summer subsurface chlorophyll maximum in the North South China Sea. PLoS One 16 (4), e0248715.

Cullen, J.J., 2015. Subsurface chlorophyll maximum layers: enduring enigma or mystery solved? Ann. Rev. Mar. Sci. 7, 207–239.

Dai, M., Guo, X., Zhai, W., Yuan, L., Wang, B., Wang, L., Cai, P., Tang, T., Cai, W.-J., 2006. Oxygen depletion in the upper reach of the Pearl River estuary during a winter drought. Mar. Chem. 102 (1-2), 159–169.

Diaz, R.J., Rosenberg, R., 2008. Spreading dead zones and consequences for marine ecosystems. Science 321 (5891), 926–929.

Fennel, K., Testa, J.M., 2019. Biogeochemical controls on coastal hypoxia. Ann. Rev. Mar. Sci. 11, 105–130.

Gan, J., Cheung, A., Guo, X., Li, L., 2009. Intensified upwelling over a widened shelf in the northeastern South China Sea. J. Geophys. Res.: Oceans 114 (C9).

Gan, J., Wang, J., Liang, L., Li, L., Guo, X., 2015. A modeling study of the formation, maintenance, and relaxation of upwelling circulation on the Northeastern South China Sea shelf. Deep Sea Res. Part II 117, 41–52.

Garcia-Robledo, E., Padilla, C.C., Aldunate, M., Stewart, F.J., Ulloa, O., Paulmier, A., Gregori, G., Revsbech, N.P., 2017. Cryptic oxygen cycling in anoxic marine zones. Proc. Natl. Acad. Sci. 114 (31), 8319–8324.

Gardner, W., Mishonov, A., Richardson, M., 2006. Global POC concentrations from in-situ and satellite data. Deep Sea Res. Part II 53 (5-7), 718–740.

Huang, L., Jian, W., Song, X., Huang, X., Liu, S., Qian, P., Yin, K., Wu, M., 2004. Species diversity and distribution for phytoplankton of the Pearl River estuary during rainy and dry seasons. Mar. Pollut. Bull. 49 (7-8), 588–596.

Kemp, W., Testa, J.M., Conley, D.J., Gilbert, D., Hagy, J.D., 2009. Temporal responses of coastal hypoxia to nutrient loading and physical controls. Biogeosciences 6 (12), 2985–3008.

Kessouri, F., McWilliams, J.C., Bianchi, D., Sutula, M., Renault, L., Deutsch, C., Feely, R. A., McLaughlin, K., Ho, M., Howard, E.M., 2021. Coastal eutrophication drives acidification, oxygen loss, and ecosystem change in a major oceanic upwelling system. Proc. Natl. Acad. Sci. 118 (21).

Kilcher, L.F., Nash, J.D., 2010. Structure and dynamics of the Columbia River tidal plume front. J. Geophys. Res. 115 (C5).

Lee, K., Matsuno, T., Endoh, T., Ishizaka, J., Zhu, Y., Takeda, S., Sukigara, C., 2017. A role of vertical mixing on nutrient supply into the subsurface chlorophyll maximum in the shelf region of the East China Sea. Cont. Shelf Res. 143, 139–150.

Li, D., Gan, J., Hui, R., Liu, Z., Yu, L., Lu, Z., Dai, M., 2020. Vortex and biogeochemical dynamics for the hypoxia formation within the coastal transition zone off the Pearl River Estuary. J. Geophys. Res. e2020JC016178.

Li, D., Gan, J., Hui, R., Yu, L., Liu, Z., Lu, Z., KAO, S.j., Dai, M., 2021. Spatiotemporal development and dissipation of hypoxia induced by variable wind-driven shelf circulation off the Pearl River Estuary: observational and modeling studies. J. Geophys. Res.

Li, X., Liu, Z., Chen, W., Wang, L., He, B., Wu, K., Gu, S., Jiang, P., Huang, B., Dai, M., 2018. Production and transformation of dissolved and particulate organic matter as indicated by amino acids in the Pearl River Estuary, China. J. Geophys. Res. 123 (12), 3523–3537. Biogeosciences.

Liu, Z., Gan, J., Wu, X., 2018. Coupled summer circulation and dynamics between a bay and the adjacent shelf around Hong Kong: observational and modeling Studies. J. Geophys. Res.: Oceans 123 (9), 6463–6480.

Lu, Z., Gan, J., Dai, M., Cheung, A.Y., 2010. The influence of coastal upwelling and a river plume on the subsurface chlorophyll maximum over the shelf of the northeastern South China Sea. J. Mar. Syst. 82 (1-2), 35–46.

Márquez-Artavia, A., Sánchez-Velasco, L., Barton, E.D., Paulmier, A., Santamaría-Del-Ángel, E., Beier, E., 2019. A suboxic chlorophyll-a maximum persists within the Pacific oxygen minimum zone off Mexico. Deep Sea Res. Part II 169, 104686.

Medina-Silva, R., de Oliveira, R.R., Pivel, M.A., Borges, L.G., Simão, T.L., Pereira, L.M., Trindade, F.J., Augustin, A.H., Valdez, F.P., Eizirik, E., 2018. Microbial diversity from chlorophyll maximum, oxygen minimum and bottom zones in the southwestern Atlantic Ocean. J. Mar. Syst. 178, 52–61.

Pasqueron de Fommervault, O., Perez-Brunius, P., Damien, P., Camacho-Ibar, V.F., Sheinbaum, J., 2017. Temporal variability of chlorophyll distribution in the Gulf of Mexico: bio-optical data from profiling floats. Biogeosciences 14 (24), 5647–5662.

Qian, W., Dai, M., Xu, M., Kao, S.-j., Du, C., Liu, J., Wang, H., Guo, L., Wang, L., 2017. Non-local drivers of the summer hypoxia in the East China Sea off the Changjiang Estuary. Estuarine Coastal Shelf Sci. 198, 393–399.

Sathyendranath, S., Stuart, V., Nair, A., Oka, K., Nakane, T., Bouman, H., Forget, M.-H., Maass, H., Platt, T., 2009. Carbon-to-chlorophyll ratio and growth rate of phytoplankton in the sea. Marine Ecol. Progress Series 383, 73–84.

Su, J., Dai, M., He, B., Wang, L., Gan, J., Guo, X., Zhao, H., Yu, F., 2017. Tracing the origin of the oxygen-consuming organic matter in the hypoxic zone in a large eutrophic estuary: the lower reach of the Pearl River Estuary, China. Biogeosciences 14 (18), 4085–4099.

Wang, G., Zhou, W., Cao, W., Yin, J., Yang, Y., Sun, Z., Zhang, Y., Zhao, J., 2011. Variation of particulate organic carbon and its relationship with bio-optical properties during a phytoplankton bloom in the Pearl River estuary. Mar. Pollut. Bull. 62 (9), 1939–1947.

Wang, Y., Wu, H., Gao, L., Shen, F., San Liang, X., 2019. Spatial distribution and physical controls of the spring algal blooming off the Changjiang river estuary. Estuaries Coasts 42 (4), 1066–1083.
Wu, K., Dai, M., Chen, J., Meng, F., Li, X., Liu, Z., Du, C., Gan, J., 2015. Dissolved organic carbon in the South China Sea and its exchange with the Western Pacific Ocean. Deep Sea Res. Part II 122, 41–51.
Wu, K., Dai, M., Li, X., Meng, F., Chen, J., Lin, J., 2017. Dynamics and production of dissolved organic carbon in a large continental shelf system under the influence of both river plume and coastal upwelling. Limnol. Oceanogr. 62 (3), 973–988.
Xing, X., Claustre, H., Wang, H., Poteau, A., Fabrizio, D.O., 2014. Seasonal dynamics in colored dissolved organic matter in the Mediterranean Sea: Patterns and drivers. Deep Sea Res. Part I 83, 93–101.
Xing, X., Qiu, G., Boss, E., Wang, H., 2019. Temporal and vertical variations of particulate and dissolved optical properties in the South China Sea. J. Geophys. Res.: Oceans 124 (6), 3779–3795.
Xu, S., Liu, Y., Fan, J., Xiao, Y., Qi, Z., Lakshmikandan, M., 2022. Impact of salinity variation and silicate distribution on phytoplankton community composition in Pearl River estuary, China. Ecohydrol. Hydrobiol. 22 (3), 466–475.
Yasunaka, S., Ono, T., Sasaoka, K., Sato, K., 2021. Global distribution and variability of subsurface chlorophyll a concentration. Ocean Sci. 1–22.
Yu, L., Gan, J., Dai, M., Hui, C.R., Lu, Z., Li, D, 2021. Modeling the role of riverine organic matter in hypoxia formation within the coastal transition zone off the Pearl River Estuary. Limnol. Oceanogr. 66 (2), 452–468.
Zhang, Z., Zhou, M., Zhong, Y., Zhang, G., Jiang, S., Gao, Y., Zhang, R., Smith Jr, W.O., 2020. Spatial variations of phytoplankton biomass controlled by river plume dynamics over the lower changjiang estuary and adjacent shelf based on high-resolution observations. Front. Marine Sci. 7, 906.
Zhao, Y., Liu, J., Uthaipan, K., Song, X., Xu, Y., He, B., Liu, H., Gan, J., Dai, M., 2020. Dynamics of inorganic carbon and pH in a large subtropical continental shelf system: Interaction between eutrophication, hypoxia, and ocean acidification. Limnol. Oceanogr.